Towards mechanical recycling of polystyrene/polypropylene blends with bottlebrush modified graphene oxide as compatibilizer

Mastooreh Seyedi, Mykhailo Savchak, Andrii Tiiara, Igor Luzinov*

Department of Materials Science and Engineering, Clemson University, Clemson, South

Carolina 29634, USA

*To whom correspondence should be addressed: e-mail: <u>luzinov@clemson.edu</u>

Abstract

The compatibilization of immiscible polystyrene/polypropylene (PS/PP) blend with virgin

graphene oxide (GO-V) and GO modified with bottlebrush reactive copolymer layer (GO-P) is

reported. This practically important blend was chosen since, currently, PS and PP are recycled to

a very low degree. The synthesized by us amphiphilic bottlebrush copolymer contained

hydrophobic and hydrophilic side chains and was attached to the GO nanosheets via epoxy

functionality. The GO modification and the introduction of GO into the blend were conducted

from water. Thus, the introduction of the compatibilizing nanomaterial can be conducted during

the mechanical recycling washing stage in a real-world situation. The final blend was prepared via

melt mixing using an extruder. We examined the influence of GO modification and the mixing

order on the blends' morphology, rheology, and mechanical properties. Thermodynamic

calculations predicted a higher interfacial activity of GO nanosheets in PS/PP/GO-P blends than

that in PS/PP/GO-V blends. The morphological and rheological study assessed this prediction. It

was demonstrated that the modified with the bottlebrush GO-P sheets were readily driven to the

PS/PP interphase. The mechanical measurements showed enhanced mechanical properties for

PS/PP/GO-P blends, especially for those in which GO was first premixed with PS.

Keywords: polymer recycling, polymer blend, compatibilization, graphene oxide, bottlebrush

Introduction

The overwhelming majority (~85%) of modern polymer materials used in industry and households are engineering thermoplastics, specifically designed not to degrade in the environment. As of 2015, roughly 6300M metric tons of plastic waste had been produced, approximately 9% of which had been recycled, 12% was incinerated, and 79% was accumulated in landfills or the natural environment. The majority (~65%) of the thermoplastic polymer materials in use are polyolefins with about an additional 5-8% of PS based materials. Those materials are recycled to a very low degree: only 0.9% of polystyrene (PS), 5.3% of low-density polyethylene (LDPE), 10.3% of high-density polyethylene (HDPE), and 0.6% of polypropylene (PP) are recycled. Current proven recycling strategies are typically divided into two major categories: mechanical and chemical recycling. As of today, the only widely used approach for large-scale treatment of plastic solid waste (such as PP, LDPE, HDPE, PS) is mechanical recycling. This recycling strategy involves: (a) the removal of contaminants through washing, (b) shredding, and (c) melting and remolding of the polymer.

Presently, the additional cost of recycling, associated with the sorting of plastic waste components, is one of the main barriers to the economic profitability of the recycled plastics industry. 13-14 The potential solution is the mechanical recycling of mixed plastic waste. 13-16 However, the significantly positive mixing enthalpy for polymer pairs usually results in the formation of immiscible blends having separated phases. 17 Those phase-separated blends typically require compatibilization since uncompatibilized polymer mixtures have a low level of interfacial adhesion and, therefore, inefficient stress transfer through the interface. 17-19 The low adhesion reduces the mechanical properties of the recycled mixed materials. Another significant challenge for generating materials with predictable and controllable physicomechanical characteristics via mechanical recycling is an "asymmetry" in melt viscosity of the blend components. In fact, numerous semicrystalline materials made of polyolefins, such as fibers and films, are fabricated from polymers having relatively low melt viscosity. 20-23 While a significant number of engineering thermoplastics (e.g., PS, ABS, high impact PS [HIPS]) have significantly higher melt viscosity. 24-26 The asymmetry causes the phase inversion point for the blend to be shifted towards the low viscosity component since high viscosity polymers tend to be a dispersed phase. 27

Effective compatibilization of an immiscible blend has to deliver (i) a decrease of the interfacial tension, causing stabilization of the dispersed phase against coalescence (which leads to a reduction in the dispersed phase size), and (ii) enhancement of adhesion between the phases in contact.^{13, 16, 19} The compatibilization can be accomplished either through chemical or physical

methods by adding small amounts of functional components. Many compatibilizers are macromolecular species with a blocky structure (e.g., block or graft copolymers), where one constitutive block is miscible with one blend component and a second block is miscible with the other blend component.¹⁶ These macromolecules can be pre-made or generated in-situ during a reactive blending process.²⁸ Also, a range of intermolecular interactions induced via the addition of functionalized (macro)molecular species can be used to increase compatibility between polymer blend components.^{13, 29} Recently, compatibilization strategies using nanoparticles and nanoplatelets have been explored to improve the mechanical properties of immiscible polymer blends.^{13,30-33} In this case, efficient compatibilization requires localization of nanomaterials at the matrix/minor phase interface, which is driven by their shape, size, chemical composition, and surface coating.

Significant efforts have been in the employment of carbonaceous materials in this compatibilization methodology since they mostly contain the same elemental composition as the polymers do, have a lower density, and can reinforce the blends in addition to the compatibilizing effect. To this end, graphene has a large π -conjugated system, making it compatible with certain polymers. 33-34 Graphene oxide (GO) is a derivate of graphene with a two-dimensional sheet of sp2 bonded carbon atoms possessing a honeycomb structure.³⁵ The oxygen-containing functional groups of GO can form physical/chemical bonding with polymer chains containing polar functional groups. For instance, GO was used to compatibilize an immiscible polyamide and polyethylene oxide blend. 15 Bai et al. employed reduced graphene oxide for the compatibilization of polystyrene/polylactic acid blends.³⁶ It has been demonstrated that the affinity of GO to nonpolar polymers, such as polyolefins, can be increased via surface modification of the nanomaterial.³⁷⁻³⁹ You et al. reported grafting PP chains onto reduced GO nanosheets and used these modified sheets to efficiently compatibilize PP/PS blends. 40 It was also found that the mixing sequence is an important fabrication parameter determining the final properties of the blends obtained. The mixing order significantly affects the level of nanofiller distribution, dispersivity, and localization in the multiphase polymer system. 41-42

To this end, we report here on the compatibilization of 80/20 PS/PP blends with virgin GO (GO-V) and GO modified with polymer layer (GO-P) to improve the blends' mechanical properties. This blend was selected since polystyrene and polypropylene are commodity polymers extensively used in various applications, which are recycled to a very low degree. We blended PP of low viscosity (melt flow index, MFI = 11.6) obtained from fibers and PS of lower MFI = 2 (higher viscosity) to model challenging real-life scenarios. The two polymers are

thermodynamically immiscible and have relatively low interfacial adhesion at the phase boundary. We found that for these highly asymmetric (in terms of viscosity) blends, PP forms a matrix, while PS constitutes the dispersed phase. To obtain GO-P, the surface of GO sheets was modified with an amphiphilic bottlebrush copolymer. GO modification has been done in water, and no organic solvent has been used in this step. The introduction of GO into the blend was also conducted from water, where PS or PP materials were suspended in water dispersion of GO and dried prior to melt-processing in an extruder. Thus, in a real-world situation, we envision that the addition of the compatibilizing nanomaterial can be conducted during the washing stage of mechanical recycling. The effect of GO and modified GO on the morphology and properties of PS/PP blends were studied. We have demonstrated that the modified with the bottlebrush GO-P sheets were driven to the PS/PP interphase and enhanced the mechanical properties of the blend. Moreover, the influence of mixing order on GO sheets' preferred localization is examined by employing two different mixing sequences.

Experiments

Materials:

PP fibers (Denier=1.5dpf, length=3mm) and PS pellets (Mw~280,000 g/mol) were supplied by Minifibers Inc. and Sigma Aldrich Inc., respectively. Graphene oxide (thickness=0.7-1.2 nm, Purity ~ 99%) suspension in water was purchased from Goographene Company.⁴⁴ According to the supplier, the size of the GO nanosheets (in XY plane) is between hundreds of nanometers to up to several micrometers. The thickness of the sheets is 0.7-1.2 nm. PS was powderized using a cryogenic tissue grinder (BioSpec products, CTGIII) before mixing with GO.

Preparation of POGL modified GO:

Poly (oligo ethylene glycol methyl ether methacrylate-glycidyl methacrylate-lauryl methacrylate) or P(OEGMA-GMA-LMA) statistical copolymer, which is denoted as POGL, was synthesized by solution free-radical polymerization as described in our preceding publication. GMA, azobisisobutyronitrile (AIBN), OEGMA (average molecular weight of 950g/mol), and lauryl methacrylate were purchased from Sigma-Aldrich. The synthesized copolymer was analyzed via Nuclear magnetic resonance (NMR, Bruker AVANCE-300). The molar and weight ratios of OEGMA:GMA:LMA monomers are ~ 0.66:0.15:0.19 and ~0.9:0.03:0.07, respectively. The molecular weight of POGL was ~ 3,000,000 g/mol, as measured by Dynamic light scattering (DLS, Malvern Zetasizer ZS) using (PS) standards. The industrially available GO suspension (5mg/ml) and POGL were mixed in a 1:2.5 mass ratio in an aqueous environment. The mixture was stirred

for four hours prior to being used for the blend preparation. We determined the amount of POGL material anchored to the GO surface using Thermogravimetric analysis (TGA 2950HR, TA Instruments) performed under nitrogen from room temperature to 600 °C at a ramp rate of 10 °C per min. For this purpose, the GO/POGL material was rinsed with water three times (to remove the unattached POGL chains) and dried in a vacuum oven. A centrifuge (Precision 100 Durafuge) was used to recover GO/POGL sheets from suspension. It was found that the GOP material is composed of ~47% GO nanosheets and ~53% of anchored POGL. We used Atomic Force Microscopy (AFM, Dimension 3100, Veeco Digital Instruments) to visualize the attachment of POGL chains onto the basal planes of GO sheets and their effect on the thickness and morphology of GO (images are not shown). The thickness of virgin GOV nanosheets was found to be ~1.1±0.1 nm. It appeared that POGL uniformly covered the GO surface. The thickness of GOP nanosheets was ~4.2 nm±0.2. Therefore, the height of the POGL layer was estimated to be about 1.5 nm.

Fabrication of PS/PP blends:

PS/PP/GO blends were prepared in three steps. In the wet processing step, PS powder and PP fibers were mixed with GO-V and GO-P suspensions in water to obtain PS/0.5wt.%GO-V, PS/0.5wt.%GO-P, PP/2wt.%GO-V, and PP/2wt.%GO-P masterbatches. The dried at room temperature polymer/GO masterbatches were extruded (CSI MAX mixing extruder, CSI Inc.) during the first melt processing step. The PP/GO and PS/GO mixtures were extruded twice at 190°C and 200°C, respectively. Pure PP and PS were also melt processed at the same conditions to avoid the influence of processing history on the properties of the blends. Finally, the PS and PP based extrudates were mixed and extruded to obtain the final blends. The resultant materials were hot-pressed (Carver hydraulic press) at 190°C for 5 minutes under 3.8MPa pressure to produce the test specimens. Consequently, PP, PP/GO, PS, PS/GO, PS/PP, and PS/PP/GO samples were fabricated. **Table 1** provides the key abbreviations for the samples used in this work.

Characterization of polymer materials

Optical microscopy (Olympus LEXT OLS 4000 confocal laser microscope) was used to observe the material's morphology. For this purpose, polymer materials were pressed to fabricate ~30μm thick films. Rheological behaviors were assessed using an XNR-400 melt flow indexer at 230°C and under 2.16Kg mass. Differential scanning calorimetry (DSC) (Model 2920; TA Instruments) was carried out at a heating/cooling rate of 20°C/min and a temperature range of -50°C to 200°C. A tensile tester (Instron, 5582) was used to measure the mechanical properties in bending mode according to ASTM D790.

Table 1. List of the fabricated samples and their compositions.

Material Abbreviation	Material Composition in wt. %			
PP	100%PP			
PP/GO-V	98%PP+2%GO-V			
PP/GO-P*	98%PP+2%GO-P			
PS	100%PS			
PS/GO-V	99.5%PS+0.5%GO-V			
PS/GO-P*	99.5%PS+0.5%GO-P			
PS/PP	80%PS+20%PP			
PS/PP-GO-V	80%PS+ 20%[PP/GO-V]			
PS/PP-GO-P*	80%PS+ 20%[PP/GO-P]			
PS-GO-V/PP	80%[PS/GO-V]+20%PP			
PS-GO-P/PP*	80%[PS/GO-P]+20%PP			

^{*} Samples also contained additional 2.5 wt parts of POGL per 1 wt part of GO.

Results and Discussion

Thermodynamics of compatibilization using GO and POGL

For GO to serve as a compatibilizer for PS/PP blend, the material has to populate the phase boundary between PS and PP. It is known that GO-V sheets containing polar functional groups have a lower affinity to non-polar PP, but they have a higher level of interaction with PS chains through the $\pi - \pi$ interactions.⁴⁵ Thus, GO-V sheets will tend to concentrate in the PS phase. To corroborate this suggestion, we employed thermodynamic relationships to estimate the possible localization of the sheets in the PS/PP blend. To this end, we calculated surface energies and their (polar and dispersive) components for in-contact pairs and determined the interfacial energies in the system using algorithms reported elsewhere.^{17, 46-48} Methodology and results are listed in **Supporting Information (SI): S1.** Next, the spreading and wetting coefficients were determined to forecast the equilibrium morphology of the PS/PP-GO-V and PS-GO-V/PP blends. **Table 2** includes the spreading and wetting coefficients for the mixtures. The spreading coefficient elucidates the likelihood of a matrix/inclusion interface to be covered with an additive in a three-component system.⁴⁹

$$\lambda_{31} = \gamma_{12} - \gamma_{32} - \gamma_{13} \tag{1}$$

where λ_{31} is the spreading coefficient for an additive to cover the PP/PS boundary, and γ_{12} , γ_{32} , and γ_{13} are the interfacial energies for PP/PS, additive/PS, and additive/PP interfaces, respectively. Component 3 (additive) is predicted to localize at the PP/PS boundary if λ_{31} is positive. Furthermore, the wetting coefficient, ω_a , has been calculated for different situations of the systems according to the following equation:⁵⁰

$$\omega_a = \frac{\gamma_{32} - \gamma_{31}}{\gamma_{12}} \tag{2}$$

The wetting coefficient detects the location of the GO sheets in the equilibrated PS/PP blends. If $\omega_a > 1$, component 3 will be located in phase 1 (PP), if $\omega_a < -1$, component 3 will be located in phase 2 (PS), and when $-1 < \omega_a < 1$, component 3 will go to the interface of phases 1 and 2. Based on the thermodynamic calculations, if the GO-V sheets are added to PS/PP blend, they will not spread over the PP/PS interface and prefer to be situated in the PS phase. Decreasing the surface energy of GO can result in nanosheet localization at the PP/PS interface. In this regard, we modified the GO sheets with the POGL copolymer (**Figure 1**) to improve the compatibilizing

ability of GO in the PS/PP blends. The polar monomer OEGMA ensures the water solubility of the macromolecules.⁵¹ GMA is insoluble in water and can react with the functional groups of GO through its epoxy groups.⁵² LMA is a non-polar monomer that balances the copolymer's polar/non-polar characteristics.⁵³ We expected this copolymer to covalent bonding with the GO sheets to coat the surface of the nanosheets. In fact, in a separate experiment, we established that intensive multiple rinsing of GO-P with a good solvent for POGL does not remove the anchored macromolecules from the GO surface.

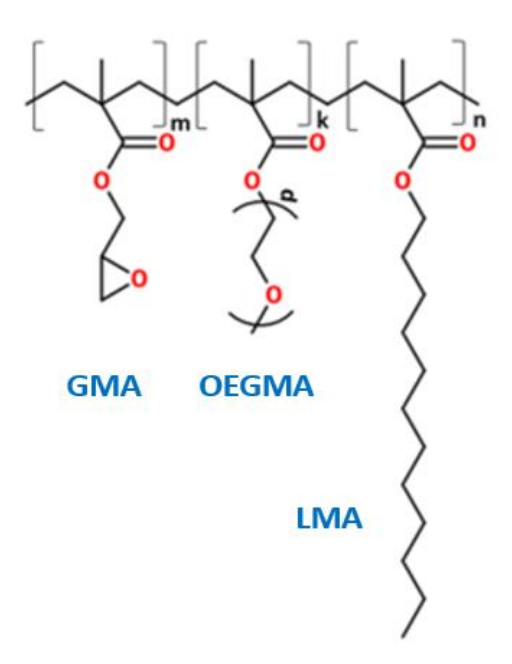


Figure 1. Chemical structure for POGL, statistical copolymer: $m \approx 0.15$, $k \approx 0.66$, $n \approx 0.19$, $p \approx 20$.

POGL is an example of molecular bottlebrushes, a special case of graft copolymers (also referred to as cylindrical polymer brushes or molecular brushes), which are linear macromolecules with relatively long side chains anchored to the backbone at high grafting densities. ^{43, 54-56} Since POGL has two types of side chains PEG and PE (polyethylene glycol of OEGMA and polyethylene/lauryl of LMA), depending on the environment the macromolecule can adopt different conformations. ⁵⁵ For instance, if PE side chains have a higher affinity to the surrounding, they are extended, while PEG chains are collapsed. The PE side chains dominate POGL interaction with polymer material in this scenario. The opposite situation is realized in the environment with a higher affinity to OEGMA chains.

Table 2. Spreading coefficient and wetting coefficients for the materials.

Material	Spreading coefficient	Wetting coefficient
PS/GO-V/PP	-73	-2.3
PS/POGL/PP and PS/GOP/PP	-6.4	-1.5
Both sides of GO-P covered with POGL		
PS/PEG/PP	-7.7	-1.5
Both sides of GO-P covered with PEG side chains		
PS/PE/PP	-0.2	0.9
Both sides of GO-P covered with PE side chains		
PS/PEG-PE/PP	3.8	0.3
Side of GO-P contacting PS covered with PEG		
Side of GO-P contacting PP covered with PE side chains		

Thermodynamic calculations (**Table 2**) show that, indeed, modification of GO with POGL macromolecules can alter the preferred localization of GO in the blend. Four main scenarios can be realized (**Figure 2**). The first one is where the surface of GO sheets is covered with POGL macromolecules without preferred conformation for the side chains (PEG and PE chains are extended or collapsed simultaneously). In that case, the GO-P sheets will migrate to the PS phase. If PEG side chains are extended over the collapsed PE chains, the GO-P will localize in the PS phase. The GO sheets covered with POGL will be situated in the PP phase if PE side chains extend and shield the PEG chains. Finally, the PE chains on one side of GO sheets can face the PP phase while the PEG chains on another side are extended toward the PS phase. Spreading coefficient and wetting coefficient calculations imply that the last situation will provide the greatest

thermodynamic prospect for the GO sheets to migrate to the PS/PP interface and cover the dispersed PP domains inside the PS matrix.

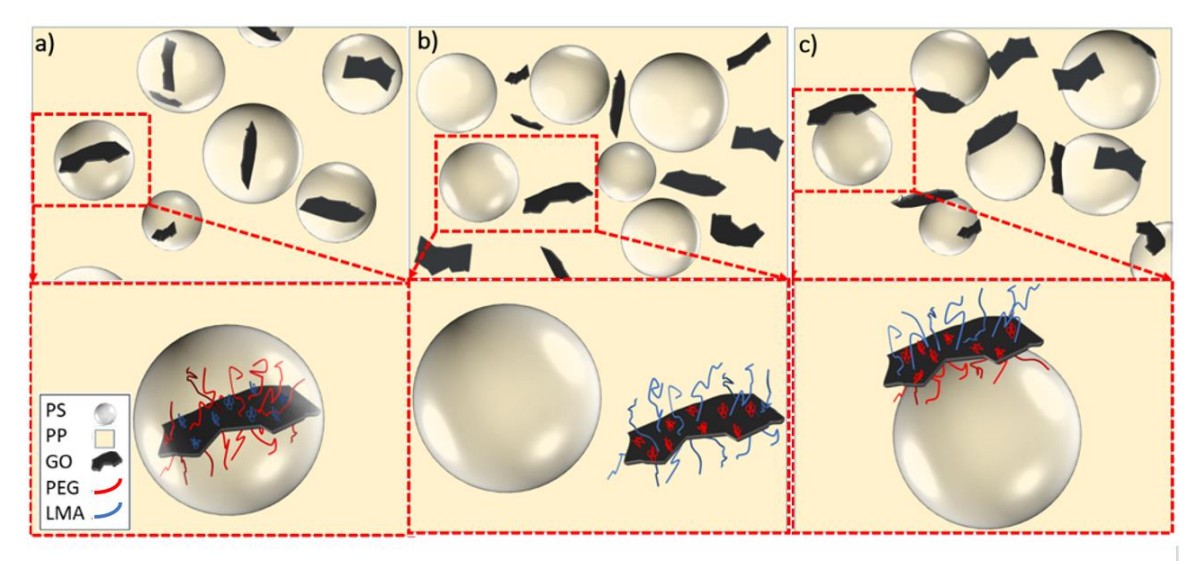


Figure 2. Schematic depicting localization of GO-P nanosheets in PS/PP blends. a) PEG side chains are covering GO-P sheets, b) PE side chains covering GO-P sheets, and c) The PE side chains face the PP phase, and the PEG side chains are contacting the PS phase.

Melt flow behavior

Along with interfacial tension, the viscosity of polymer blend components is a critical parameter that influences the phase dispersion and the localization of fillers. To this end, we measured the melt viscosities of the materials involved and their mixtures using a capillary rheometer (SI: S2). The viscosity data are presented in Table 3.

Effect of GO addition

The viscosity of phases and blends is significantly increased by GO sheets' presence (**Table 3**). It is expected since the addition of (nano)filler is generally shown to increase the viscosity of polymer melts via the polymer/surface interactions leading to the interphase formation in the vicinity of the filler.^{36-37, 45, 57-61} Higher filler's surface area and level of interaction cause a greater increase in the melt viscosity. At relatively low filler content, the influence of nanofiller on the viscosity can be fitted to Einstein type equation:^{59, 61}

$$\eta_r = 1 + [\eta] \varphi + k([\eta] \varphi)^2 \tag{3}$$

where relative viscosity, η_r is the ratio between viscosities of filled and neat polymer material, φ is filler content, $\lceil \eta \rceil$ and k are apparent intrinsic viscosity and interaction constant, respectively.

Stronger interaction between nanofiller and polymer is quantified by increasing $[\eta]$ and k. Our data shows that GO-V and GO-P interact differently with the polymers constituting the blends, where the highest relative viscosity of 2.2 is observed when GO-V is mixed with PP. Hence, GO-V interacts with the PP matrix to a higher extent than with PS material. This trend is not observed for GO-P, where the level of interfacial interaction for both polymers is practically the same. We associate this observation with the shielding of the GO surface by the anchored POGL shell. It is necessary to point out that the relative viscosity is quite close for PS/GO-V and PS/GO-P, indicating that the GO-V and GO-P materials interact with PS to virtually the same extent. For the blends, a different tendency was found. The relative viscosity is significantly higher for the blends containing GO-P in comparison to η_r observed for PP/GO-P and PS/GO-P materials. We associate this finding with a significant localization of GO-P at the PP/PS interface, as predicted by the thermodynamic calculations above. Conversely, η_r increase was not observed for the blends containing GO-V. For PS/PP-GO-V, a decrease in the viscosity is found. This observation suggests a certain migration of GO-V from the PP phase to PS as forecasted by the thermodynamical estimations.

Table 3. Viscosity data for the materials and size of blend's dispersed phase.

Material	Viscosity (Pa s)	Predicted blend viscosity by Eq. 4 (Pa s)	Relative viscosity calculated by Eq. 3	η _d /η _m Eq. 5	Diameter of PS domains (µm)
PP	625				
PP/GO-V	1368		2.2		
PP/GO-P	815		1.3		
PS/PP	657	2692		6.5	6.4
PS/PP-GO-V	1205	3198	1.8	3	4.3
PS/PP-GO-P	1348	2854	2.1	5	5.4
PS-GO-V/PP	1019	3767	1.6	10	5.7
PS-GO-P/PP	1473	3555	2.2	9.3	3.9
PS/PP-POGL	1205				
PS	4064				
PS/GO-V	6252		1.5		
PS/GO-P	5805		1.4		

The viscosity of the blends

The overall viscosity of an immiscible polymer blend depends on the viscosity of its components, phase morphology, and interfacial interactions. The interactions can be examined via log-additive rule: 16, 27, 62

$$log(\eta) = \Sigma_i \varphi_i \, log(\eta_i) \tag{4}$$

where φ_l and η_l are volume fraction and viscosity of component i, respectively. The blends are characterized by four major categories: additive blends following Eq. 4, blends with positive or negative deviation from the log-additivity, and blends that exhibit both positive and negative deviations (typically when their phase structure changes). The positive deviation is observed for the blends with strong interfacial interaction, while the opposite effect is observed when interactions are weak. We calculated viscosities for the blends using the log-additive rule (**Table 3**), and for all blends prepared, there is a negative deviation from the rule. The highest deviation is for the neat PS/PP blend. In fact, the PS/PP viscosity is only slightly higher than the viscosity of the low viscosity component, PP. This behavior was previously reported for PS/PP blends, where PS had a significantly higher viscosity than PP.⁶³ Adding GO-V and GO-P enhanced the blend viscosity significantly, which indicates the interfacial activity of the GO additives. ¹⁶ GO-P brings viscosity somewhat closer to the additive rule and, therefore, the sheets modified with POGL bottlebrush have the higher interfacial activity.

Effect of GO-V on PS/PP blend

Morphology

Figure 3 shows the optical microscopy images of PP-GO-V and PS-GO-V masterbatch mixtures. The GO-V sheets are clearly visible at a micrometer scale in the mixtures. It is necessary to point out that, since the size of the GO sheets used in this work ranges (in XY plane) between hundreds of nm to several microns, only the larger micron-scale sheets can be observed in the optical microscope. At the higher magnification, the nanosheets appear to be crumpled, wrinkled, and (to some extent) aggregated. We associate this observation with high interfacial tension at the PP/GO-V interface (**SI: S1**) and the semicrystalline nature of PP. Indeed, during crystallization, the GO-V sheets are forced into amorphous regions of the material. The sheets are less packed in PS-GO-V masterbatch, and single sheets can be observed in the PS matrix (**Figure 3**). The nanosheets also do not appear to be significantly aggregated and wrinkled. This observation can be connected to

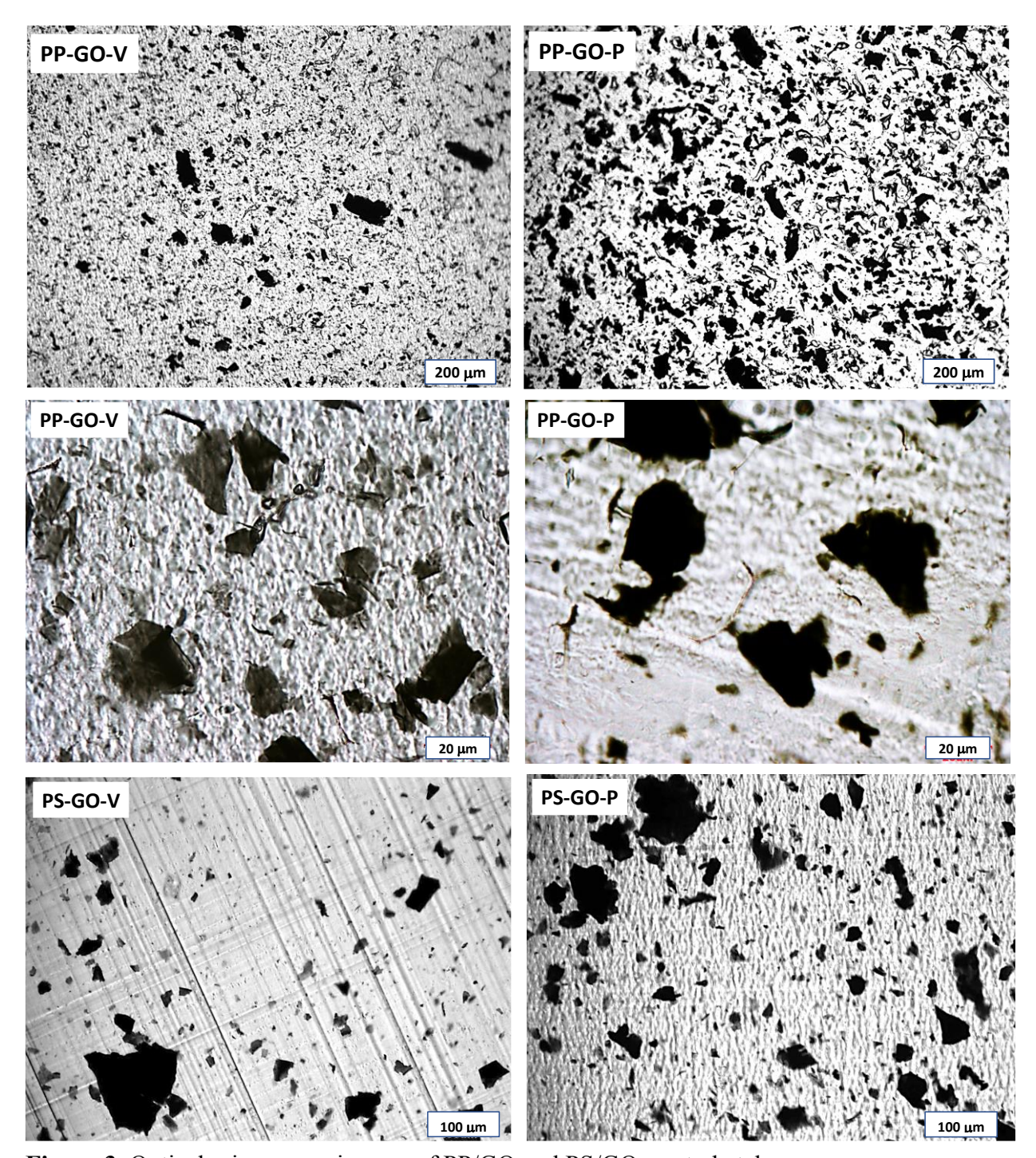


Figure 3. Optical microscopy images of PP/GO and PS/GO masterbatches.

the lower GO-V concentration in PS, the PS amorphous nature, and lower PS/GO-V interfacial tension.

Figure 4 shows the optical microscopy images of PS/PP, PS-GO-V/PP, and PS/PP-GO-V blends. As expected, the immiscibility of PS and PP results in phase separation, where one phase

is continuous, and another phase is dispersed. Even though PP is a minority phase in our blends, it is not obvious that PP constitutes the dispersed phase. Here, the ratio between the melt viscosities of the polymers blended is an important factor to consider. Namely, in a polymer/polymer mixture at a certain concentration of phase inversion, the dispersed phase becomes the matrix and vice

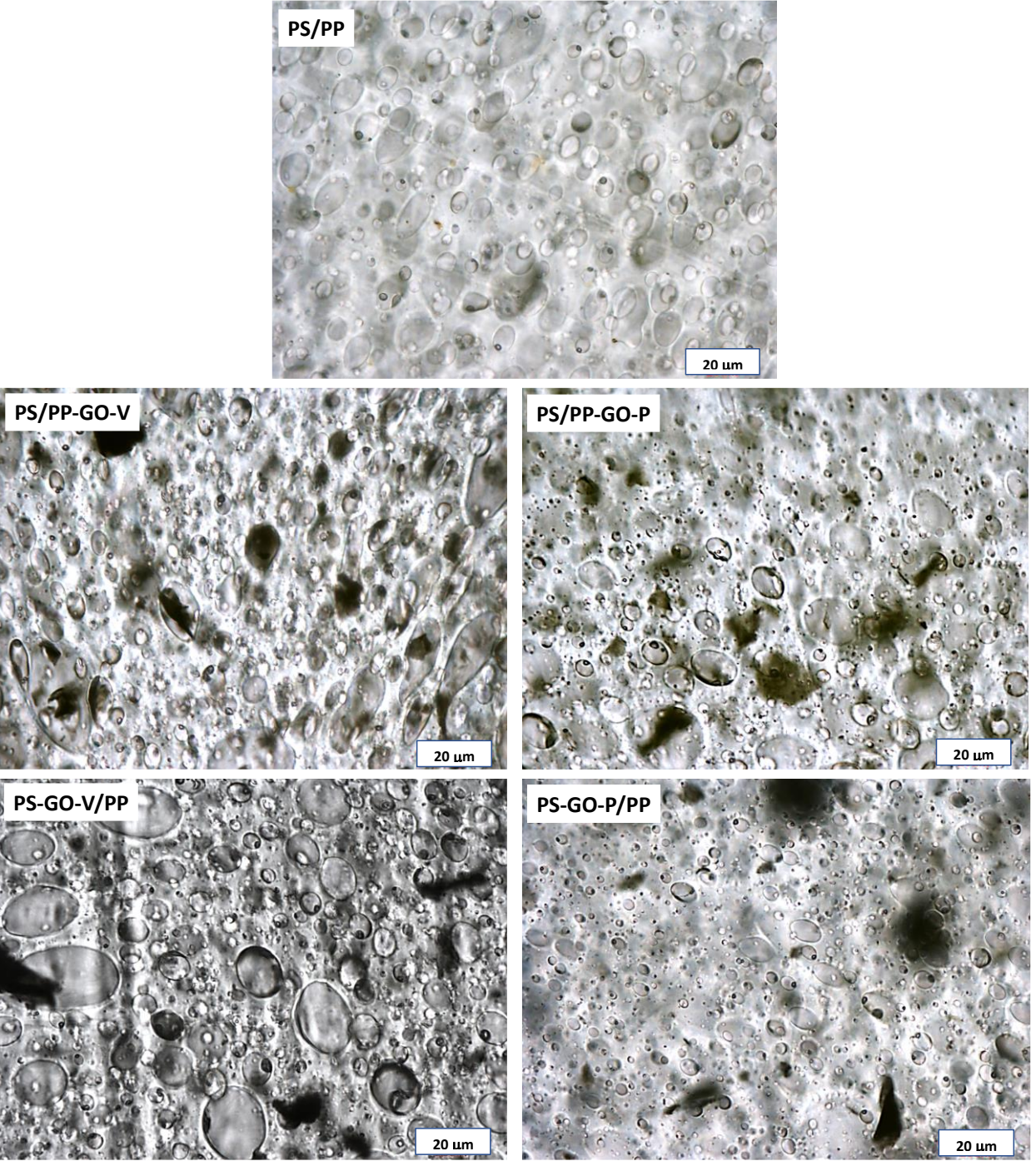


Figure 4. Optical microscopy images of PS/PP and PS/PP/GO blends.

versa.^{27, 62, 64} A number of models have been developed to approximate the phase inversion composition. These models have been applied to different polymer blend systems without leading to a universal rule since phase morphology found in polymer blends significantly depends on mixing time and conditions, interfacial modifiers, and the type of blenders/extruders used.⁶⁴ In general, in the vicinity of phase inversion concentration phase co-continuity can be observed as volume fraction (φ) of minority low viscosity polymer is near the percolation threshold ($\varphi \approx 0.16$).²⁷ The middle range of concentrations, at which phase co-continuity is found, can be roughly estimated, for instance, by Paul and Barlow's empirical equation:⁶⁵

$$\varphi_{2inv} = 1/(1 + \eta_1/\eta_2) \tag{5}$$

where φ_{2inv} is the volume fraction of blend's component 2 at the middle of the co-continuity region and η_1 and η_2 are melt viscosities of components 1 and 2, respectively.

We determined φ_{2inv} for the polymer blends studied here (**SI: S3**). For all blends, but PS/PP-GO-V, φ_{2inv} is significantly lower than 0.22 (volume fraction of PP), indicating that PP should be the matrix and highly viscous PS should form the dispersed phase. To investigate the morphology of the blends further, we conducted a solvent test. Specifically, we immersed the blend samples into toluene, a selective solvent for the PS phase.⁶⁴ All samples tested were not disintegrated after the solvent extraction, indicating that the PP phase is continuous (**Figure 5**).

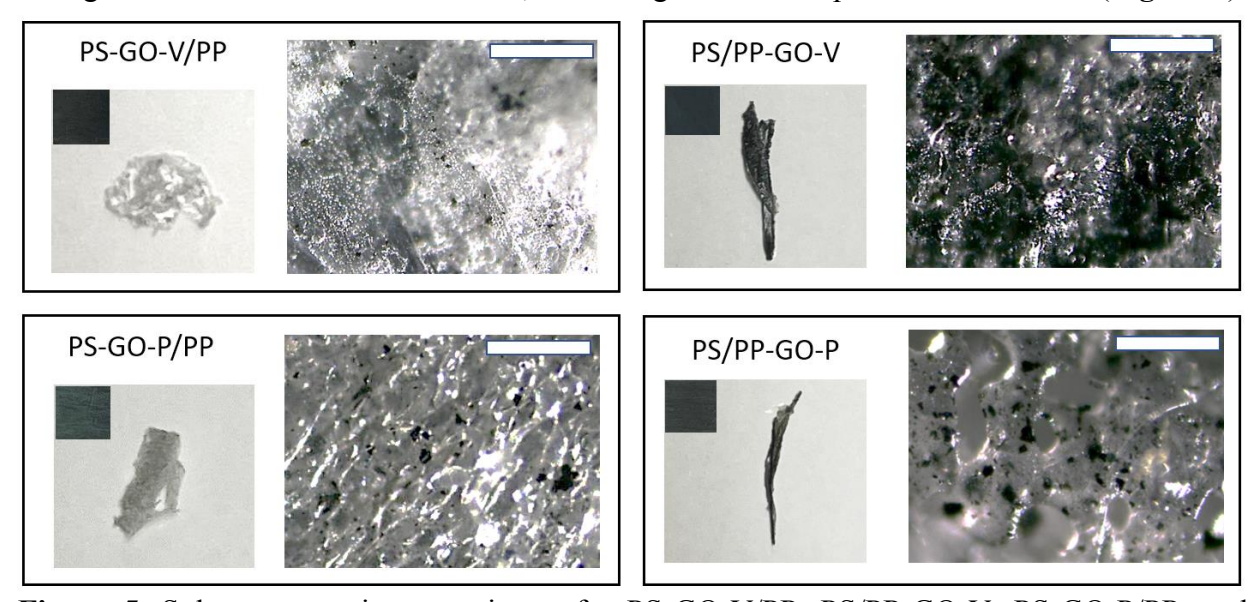


Figure 5. Solvent extraction experiment for PS-GO-V/PP, PS/PP-GO-V, PS-GO-P/PP, and PS/PP-GO-P blends. For each sample: the dark squares are the samples before the extraction test, the photographs are the samples after extracting the PS phase, and the optical microscopy images of the remained materials show level of GO residue in the PP phase. The scale bar is 200 μ m.

The result suggests that in the case of PS/PP-GO-V, where calculated $\varphi_{2inv} = 0.26$, a GO-V migration to the PS phase occurred. It appeared that the relocation raised the viscosity of the PS phase and reduced the viscosity of the PP phase, causing $\varphi_{2inv} < 0.22$. In fact, the certain localization of GO-V in the PS dispersed phase can be observed (**Figure 4**). Our thermodynamic estimations predicted this redistribution. The images of the PP phase that remained after the solvent extraction experiments provide additional information on the GO-V distribution (**Figure 5**). It is apparent that a significant number of GO-V sheets are still present in the PP phase since thermodynamic equilibrium can not be reached during a short time of mixing in an extruder. Also, as indicated by the viscosity measurements, PP macromolecules actively interacting with the GO-V surface and adsorption of the macromolecules on the nanosheets can delay/prevent their transfer into the PS phase. For the PS-GO-V/PP blend, significant migration of GO-V into PS was not observed (as predicted by the wetting coefficient), **Figure 5**.

The dispersed PS phase's size is measured for 100 inclusions in each sample, and the size and size distributions are shown in **Table 3 and SI: Figure S1**. After comparing PS/PP blend and PS/PP/GO-V blends, it can be concluded that the size of these domains somewhat decreases in the presence of GO sheets. For polymer blend with dispersed morphology, the size of the inclusions is a function of the component content, their viscosity, and interfacial tension:⁶⁶

$$d = \frac{4\gamma \left(\frac{\eta_d}{\eta_m}\right)^{0.84}}{G\eta_m} \qquad \text{for p > 1} \qquad \text{and} \quad d = \frac{4\gamma \left(\frac{\eta_d}{\eta_m}\right)^{(-0.84)}}{G\eta_m} \qquad \text{for p < 1} \qquad (6)$$

where γ is interfacial tension, d is the number average particle diameter, G is the shear rate, η_m is the melt viscosity of the matrix, η_d is the melt viscosity of the dispersed phase, and p (η_d/η_m) is the viscosity ratio. In our case p > 1, thus with a decrease of η_d/η_m size dispersed phase has to decrease if interfacial tension does not change. The data for η_d/η_m calculated based on the measured viscosities is presented in **Table 3**.

The spreading/wetting coefficients (**Table 2**) predict that GO-V does not have a thermodynamic tendency to occupy the blend's interface. Therefore, it can be suggested initially that for PS/PP, PS-GO-V/PP, and PS/PP-GO-V interfacial tension is close. Accordingly, the smallest size for PS inclusions is observed for PS/PP-GO-V blend having the smallest predicted value of η_d/η_m . The size of PS droplets in the PS-GO-V/PP blend has to be the largest because of the highest η_d/η_m value. Nevertheless, in this case, the size of the inclusions is somewhat smaller than that for the PS/PP material. Thus, as already indicated by the values of the blend viscosity,

GO-V has certain interfacial activity in the blends. The formation of a transition zone at the PS/PP interface by GO sheets to decrease the thermodynamically unfavorable contacts can be in accordance with the "slim-fast mechanism" theory. The theory predicts that nanosheets have a specific ability to cover significant parts of the interface to effectively protect two opposing blend polymers from each other. It also can be suggested that, in the course of the melt mixing, selected GO-V sheets can adsorb PS chains on one side and PP chains on another side and attain the ability to decrease interfacial tension in the system. GO surface is shown to be inhomogeneous, where about half of the GO surface contains different types of C-O linkages, and the other half are C-C bonds. Thus, many non-oxidized areas on the GO surface have a higher affinity to PP macromolecules.

Thermal transitions

Differential Scanning Calorimetry (DSC) results for PP, PS, PS-GO-V, and PP-GO-V materials are shown in **Table 4 and SI: Figures S2-S3**. Samples were first heated from -50 °C to 200 °C to erase their thermal history. DSC results indicate that the addition of GO-V to PP causes minor (3-5 degrees) increase in crystallization and melting temperatures (T_c and T_m) of the material. Thus, the nanosheets act as additional heterogeneous nucleation sites that initiate the formation of thicker lamellas constituting semicrystalline spherulites. ^{17,37} In contrast, PP-GO-V has a lower degree of crystallinity (decrease of 4%) than pure PP. We associate this observation with the ability of GO-V sheets to arrest physically growth of larger spherulites. The DSC measurements (**Table 4**) also demonstrate that the addition of GO-V (at 0.5 wt parts) to PS does not alter its glass transition temperature (T_g). Thus, the mobility of PS chains in the material is not restricted by GO-V nanosheets.

Table 4 and SI: Figure S4 display DCS results for PS/PP, PS-GO-V/PP, and PS/PP-GO-V blends. There is no significant change in T_g of PS and T_c/T_m of PP for those blends compared to pure PS and PP, respectively. However, for the blends, the distribution of the lamella thicknesses is wider, as indicated by broadening the melting peaks in the blends. The degree of crystallinity of PP in the PS/PP blend is ~7% higher than the one observed for pure PP, indicating that surface of PS droplets can serve as additional heterogeneous nucleation sites. However, the addition of GO-V considerably reduced the degree of crystallinity of the PP phase. The decrease of about 10% is

more pronounced than the one for PP-GO-V material (4% decrease). Thus, in the blend, GO-V sheets interfere with the spherulite growth.

Table 4. Thermal properties of PP, PS, and PS/PP composites.

Sample		PP melting and crystallization				
	Tg of PS	Tm	ΔHm (J/g)	Degree of crystallinity	Tc	
PP		158	97	0.47	113	
PP/GO-V		161	88	0.43	118	
PP/GO-P		160	71	0.35	115	
PS/PP	103	155	21	0.51	113	
PS/PP-GO-V	105	156	17	0.41	114	
PS/PP-GO-P	104	155	13	0.31	113	
PS-GO/PP	103	156	17	0.40	114	
PS-GOP/PP	103	157	16	0.37	114	
PS	104					
PS/GO-V	104					
PS/GO-P	103					

It is well established that the crystallization behavior of a crystallizable polymer in a polymer blend depends on the phase morphology of the material. To this end, Omonov et al. studied in detail the crystallization of polypropylene in PS/PP blend as a function of the blend morphology. It was found that if PP is a continuous phase, the nucleation is heterogeneous, and T_c is close to the one observed for the pure PP. If PP forms a dispersed phase, the droplet volume limits the nucleation mode. The material demonstrates comparable crystallization peaks connected to heterogeneous nucleation and homogeneous nucleation at a much lower temperature ($\sim 76\,^{\circ}$ C in their study). In our case, we observed predominantly heterogeneous nucleation (SI: Figure S4), since the major crystallization peak is close to the T_c of pure PP. We did observe a small peak of homogeneous nucleation at $\sim 50\,^{\circ}$ C. This result shows that some small amounts of PP can be located in PS droplets.

Mechanical properties

To evaluate the mechanical properties of the materials studied here, we conducted a three-point bending flexural test. First, we determined the influence of GO-V on pure PP and PS materials (**Figure 6**). We expected an increase in the moduli of the materials since the elastic modulus of

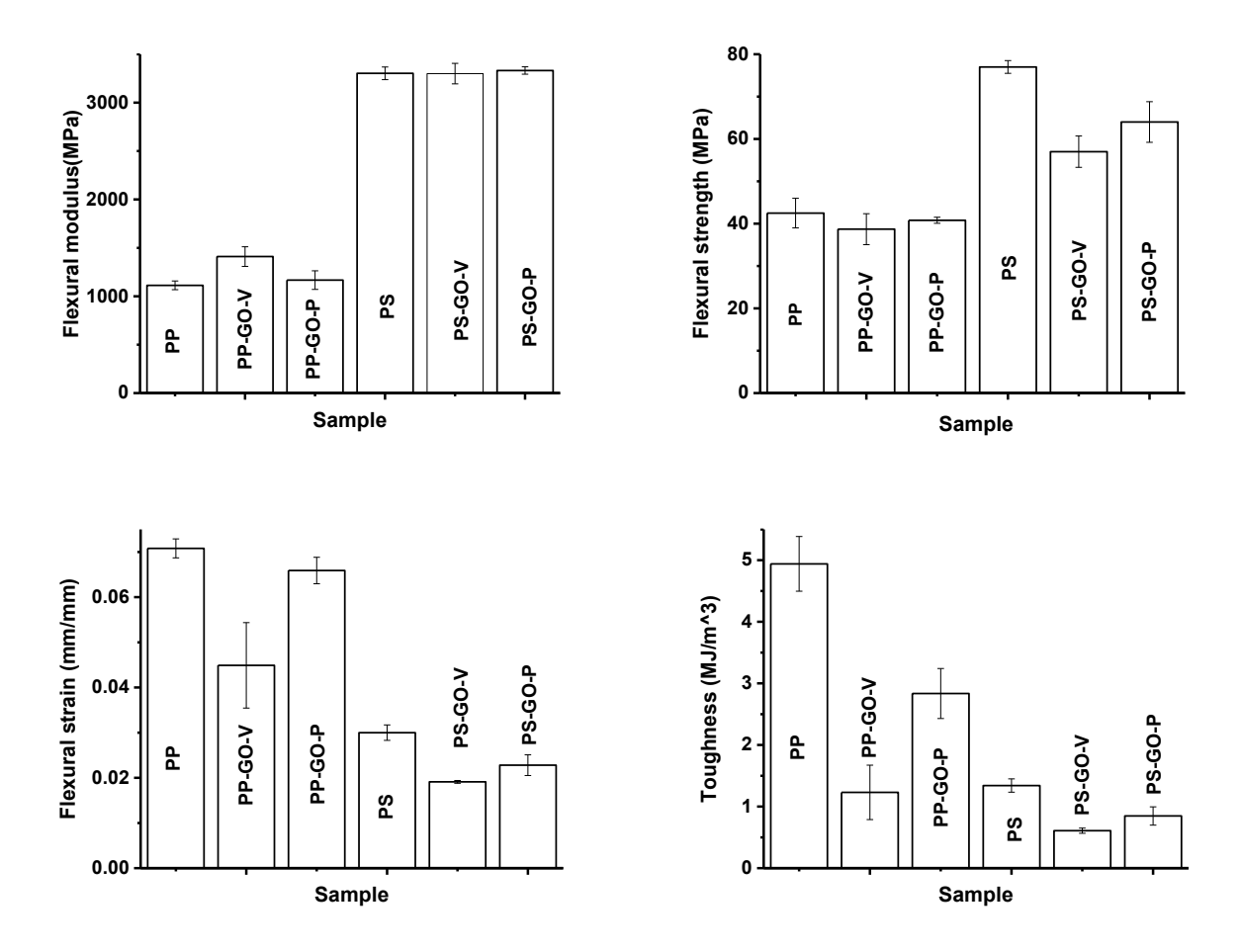


Figure 6. Mechanical properties of PP and PS materials derived from three-point bending test.

GO is reported to be ~ 0.25 TPa (2-4 orders of magnitude higher than the modulus for engineering polymers). 68-70 In fact, the flexural modulus of PP/GO-V increased by about 25% compared to pure PP. However, the addition of GO-V to PS virtually did not change the moduli of the material. First, the increase for PP/GO-V is observed due to the higher amount of embedded GO. Additionally, it is reported that an increase in the (experimentally measured) modulus for the composites containing graphene-based material is higher for polymers with a lower modulus. 66 The flexural strength just slightly decreased for the PP-GO-V compared to virgin polymer. This decrease is more pronounced for PS-GO-V. Flexural strain at maximum and toughness of the materials decreased to a much higher degree. Specifically, the strain and toughness decreased by more than 30% (~37% for PP and ~33% for PS) and 50% (~75% for PP and ~ 55% (for PS), respectively. This decrease has been reported previously for PP composites reinforced with GO. The results have indicated that the polymer chains' segmental mobility is restricted due to their

interaction with GO sheets. The decrease in the mobility of the macromolecules leads to higher modulus and lower toughness/deformation limit.

The results obtained from the three-point bending measurements for the blends are summarized in **Figure 7**. Due to the thermodynamic immiscibility of PS and PP, PS/PP blends

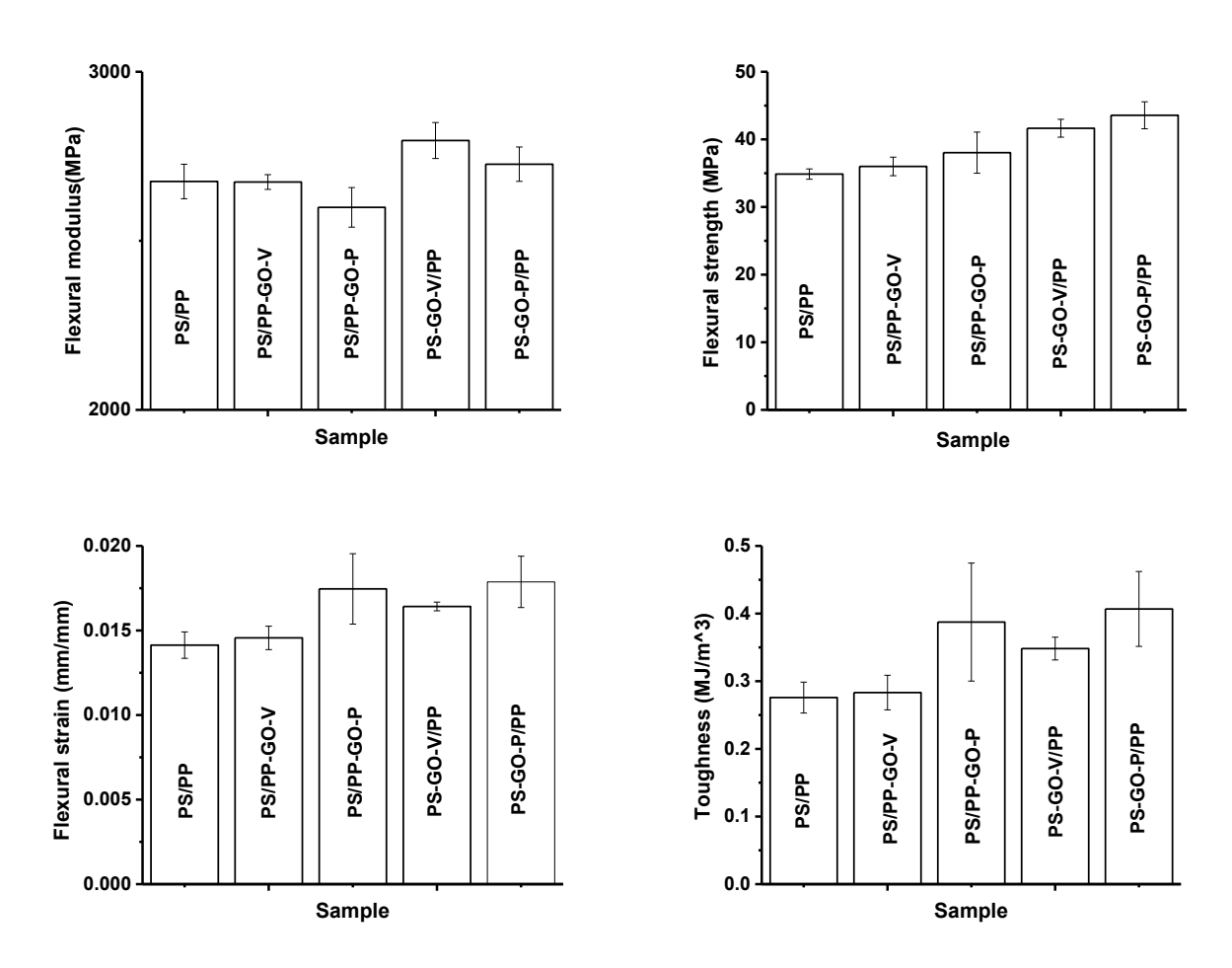


Figure 7. Mechanical properties of PS/PP blends obtained from three-point bending test.

are expected to demonstrate negative deviation from an ideal mixing (additive) rule in terms of mechanical properties since the PS/PP blends interface acts as a mechanical defect. ^{16-17, 19, 33} The mixing rule prediction for the PS/PP blend are presented in **Table S7 (SI: S4)**. Thus, we report the influence of GO addition on mechanical properties in terms of (a) level of negative deviation from PS/PP ideal (mixing rule) behavior and (b) direct comparison of the mechanical behavior of PS/PP/GO with that of uncompatibilized PS/PP blend.

The flexural moduli of the PS/PP and PS/PP/GO-V blends are negligibly (2-6%) lower than the values predicted by the mixing rule for PS/PP blend. Those changes are within

experimental error. The flexural strength and strain of the PS/PP and PS/PP/GO blends demonstrate significant (40-50% strength and 57-63% strain) negative deviation from the mixing rule. However, the addition of GO to the blend somewhat improves the values of these parameters. The lowest deviation (40% strength and 57% strain) is recorded for the PS-GO-V/PP blend. The addition of GO-V to the PS phase prior to the blend formation increases the strength and strain by 9% and 16% compared to PS/PP material, respectively. Obviously, the same pattern is observed for the toughness (calculated from flexural strength and strain), where the PS-GO-V/PP blend toughness is 25% higher than the toughness of the PS/PP blend.

Our findings confirm the positive effect of GO-V on the affinity between PP and PS phases. Mechanical testing, along with the (above-mentioned) viscosity results, indicates significant localization of GO-V at the interface, which has a compatibilizing effect on the PS/PP blend. The localization is more efficient when GO-V is premixed to the PS phase. In contrast to the observed results, the thermodynamical calculations showed that pristine GO-V would locate inside the PS phase. However, our calculations employ the notion of uniformity of GO surface. In reality, about half of the GO surface contains different types of C-O linkages, and the other half are C-C bonds⁶⁷, confirming that there is a notable amount of non-oxidized areas on GO that can be tended to the PP phase.

Effect of POGL addition to PS/PP blend

Before adding the GO sheets modified with POGL to PS/PP blend, we examined the impact of POGL addition on the mechanical properties of the blends (SI: S5, Figure S5). Specifically, 80PS/20PP/1POGL weight parts blends were fabricated. The amount of added POGL was the same as was used to prepare PS/PP/GO-P blends. The preceding experiment established that POGL is immiscible with PP and PS since PP-POGL and PS-POGL are phase-separated materials (results not shown). We found that the order of POGL addition to a blend has a vital impact on the mechanical properties. When the bottlebrush is added to the PS phase prior to the PS-POGL/PP blend fabrication, the presence of POGL significantly decreases flexural modulus (~16%) and increases flexural strain (~21%) compared to the unmodified PS/PP blend. The POGLE incorporation does not change the flexural strength. In the case of the bottlebrush premixing with the PP phase, the mechanical behavior of the PS/PP-POGL blend is completely different. The modulus does not change, while the strength and strain significantly increase. Namely, the strength

and strain increase by $\sim 16\%$ and $\sim 43\%$. The obtained results indicated that POGL is capable of modifying PS/PP interface and, to a certain extent, compatibilize the blend. The localization of POGL at the interface was also corroborated by the decrease of the average size of PS inclusions in the presence of POGL from ~ 6.4 to ~ 5 microns (SI: S6). Interestingly, the size of the PS droplets is not dependent on the order of the bottlebrush addition.

The strong dependence of the mechanical properties on the premixing order indicates that the molecular bottlebrush adopts different interfacial conformations depending on the order. We associate this phenomenon with the dissimilarity in macromolecules' initial conformation in the PS and PP materials prior to the blend fabrication. Based on the thermodynamical affinity signified by the interfacial tension (SI: S1), the alkyl subchains of the LMA monomeric units are exposed at the POGL/PP interface in the PP phase. In the PS phase, PEG subchains occupy the POGL/PS interface. When PS is mixed with PP, the lowest energy conformation for POGL at the interface is when the alkyl subchains are exposed to the PP phase, while the PEG subchains protrude into the PS phase. We suggest that the reorientation of POGL during rapid (non-equilibrium) melt mixing is more efficient from the PP phase. Indeed, given that LMA is a minority component, PEG subchains of OEGMA (majority component) can promptly reach the PS phase during the mixing. While in the PS phase, where POGL/PS interface is occupied with the PEG subchains, it is more changing for the alkyl subchains to reach the PE/PS interface.

Effect of GO-P Addition to PS/PP blend

Morphology

Figure 3 displays the optical microscopy images of PP-GO-P and PS-GO-P masterbatch mixtures. It is obvious that the modified with the bottlebrush GO-P sheets are dispersed considerably better than GO-V ones in the PP matrix. This observation is in accord with the thermodynamic predictions (**Table 1**). Indeed, interfacial tension for the GO-P/PP interface is significantly lower than that predicted for the GO-V/PP one (**SI: S1**). The individual GO-P sheets are clearly visible in the PP-GO-P masterbatch mixture at a micrometer scale. We did not observe significant aggregation and crumbling of GO-P dispersed in PP. **Figure 3** also shows that individual GO-P nanosheets are well distributed (without significant aggregation) in the amorphous PS matrix.

The optical microscopy images of PS/PP, PS-GO-P/PP, and PS/PP-GO-P blends are displayed in **Figure 4**. The materials have phase-separated morphology and, according to

calculated φ_{2inv} for the polymer blends using **Eq. 5** (**SI: S3**), PP constitutes the matrix since φ_{2inv} < 0.2. We carried out the solvent test⁶⁴ and confirmed that the blends were not disintegrated after the toluene extraction, indicating that the PP phase is continuous (**Figure 5**). It is challenging to determine the distribution of GO-P between blend's phases from images presented in **Figure 4**. Better information is provided by the optical images of the PP matrix after the solvent extraction (**Figure 5**). Specifically, we found that GO-P migration from PP to PS (for PS/PP-GO-P) and from PS to PP (for PS-GO-P/PP) is more pronounced than the migration for the blends containing GO-V. We associate this phenomenon with the ability of POGL chains to reorient, expressing alkyl side chains in PP and PEG side chains in PS.

Table 3 and SI: Figure S1 show the size of the PS phase in PS-GO-P/PP ($\sim 3.9 \mu m$) and PS/PP-GO-P ($\sim 5 \mu m$) blends. As in the case of the blends containing GO-V, the size of the PS domains does not correlate directly with the η_d / η_m ratio (Table 3). Thus, according to Eq. 6, interfacial tension at PS/PP interface decreases significantly with the presence of GO-P compared to PS/PP blends. The lowest interfacial tension value is for the PS-GO-P/PP blend, where the nanosheets covered with POGL are premixed with the PS phase. Thus, as predicted by thermodynamical calculations, POGL material absorbed on GO nanosheets can rearrange at the interface, presenting a significant number of alkyl chains to the PE phase and PEG moieties to PS. During a limited time of the melt mixing, the rearrangement is the most efficient when GO-P is premixed with PS. We associate this observation with (a) highly thermodynamically unfavorable PP/PEG contact ($\gamma = 12 \text{ mN/m}$) in comparison to less unfavorable PS/alkyl contact ($\gamma = 6 \text{ mN/m}$) and (b) highly thermodynamically favorable PP/alkyl contact ($\gamma = 0.5$ mN/m) in comparison to less favorable PS/PEG contact ($\gamma = 2.1 \text{ mN/m}$), SI: S1. It emerges that the rearrangement for GO-P located in the PS phase (presenting largely PEG moieties at the surface) is more efficient than that for the nanosheets situated in the PP phase (exhibiting mostly alkyl sub-chains to the boundary).

Thermal transitions

DSC data for PS-GO-P and PP-GO-P materials are shown in **Table 4 and SI: S4**. The results demonstrate that the addition of GO-P to PP causes a lower degree change in T_c and T_m of the material compared to GO-V addition. Therefore, the POGL shell effectively screens the GO surface and does not cause additional heterogeneous nucleation. It is noticeable that PP-GO-P has

a significantly lower degree of crystallinity than pure PP and PP-GO-V. As for the GO-V, we connect this finding to GO-P sheets' ability to physically arrest the growth of larger spherulites (**Figure 4**). The larger decrease in crystallinity can be associated with better dispersivity of GO-P in the PP matrix. The DSC results also show that the addition of GO-P (at 0.5 wt parts) to PS does not change its glass transition temperature (T_g). Thus, the mobility of PS chains in the material is not restricted by GO-P nanosheets.

DCS results for PS-GO-P/PP and PS/PP-GO-P blends are shown in **Table 4 and SI: S4**. As for the GO-V addition, there is no significant change in T_g of PS and T_c/T_m of PP for those blends compared to pure PS and PP, respectively. Analogously, widening of the melting peaks is observed for the PS-GO-P/PP and PS/PP-GO-P materials, indicating broadening the distribution of the lamella thicknesses. The degree of crystallinity of PP in the PS-GO-P/PP and PS/PP-GO-P blend is lower than the one observed for the pure PP/PS blend. The decrease is higher for PS/PP-GO-P (~20% decrease) than for PS-GO-P/PP (~ 14% decrease). Thus, as for GO-V containing materials, the GO-P nanosheets impede the spherulite growth. The effect on the degree of crystallinity is more pronounced when GO-P is preblended with PP prior to the blend formation. For GO-P containing materials, the extent of homogeneous nucleation is even lower than that for other PS/PP blends discussed in this work. Hence there is no significant amount of PP material inside PS droplets.

Mechanical properties

To begin with, we measured (in a three-point bending flexural test) how the addition of GO-P to pure PP and PS (**Figure 6**) affects their mechanical properties. We note a significant difference in mechanical properties between PP-GO-P and PP-GO-V materials. Namely, the addition of GO-P to the PP matrix does not significantly influence its mechanical properties in terms of flexural modulus, strength, and strain. As a result, the decrease of PP-GO-P toughness is considerably lower than that for PP-GO-V. We connect this finding to the ability of POGL, enveloping the nanosheets, to effectively shield the GO surface from interaction with PP macromolecules. Also, a decrease in the degree of crystallinity of the PP matrix can contribute to the increased ductility of PP-GO-P compared to PP-GO-P material. As in the case of GO-V addition, the flexural modulus of PS is not influenced by the addition of 0.5% of GO-P. Analogously, the flexural stress, strain, and toughness are decreased by the addition. However, this decrease is to a lower degree.

Figure 7 displays the three-point bending measurements for the blends containing GO-P. The results are considered in terms of (a) level of negative deviation from PS/PP ideal (mixing rule) behavior (SI: S4, Table S7) and (b) direct comparison of the mechanical behavior of PS/PP/GO-P with that of uncompatibilized PS/PP blend and PS/PP/GO-V blends. The flexural moduli of the PS/PP/GO-P (as those for PS/PP and PS/PP/GO-V) are insignificantly lower (2-4%) than predictions of the PS/PP mixing rule. The flexural strength and strain of the PS/PP/GO-P blends also demonstrate (~ 38-45% strength and 54-55% strain) negative deviation from the mixing rule. Nevertheless, the addition of GO-P to the PS/PP blend definitely improves the strength and strain demonstrated by the blend. The lowest negative deviation among PS/PP, PS/PP/GO-V, and PS/PP/GO-P materials for flexural strength (38%) and strain (54%) is shown by PS-GO-P/P. Thus, the preblending of GO-P with PS increases the strength and strain by $\sim 25\%$ compared to PS/PP material. The toughness of PS-GO-P/PP is 48% higher than the toughness of PS/PP material. Obviously, the pre-localization of GO-P in the PP phase does not offer the same level of improvement. As we compare all blends studied here in terms of mechanical properties in all categories (but one), PS-GO-P/PP material demonstrates the best mechanical characteristics. Only in the flexural strain category, PS/PP-POGL material is somewhat better.

Conclusions

We demonstrated that PS/PP blend can be efficiently compatibilized via the addition of GO modified with an amphiphilic bottlebrush copolymer layer. The compatibilization occurs via migration of GO-P to the PS/PP interface as forecasted by thermodynamic estimations. Specifically, the addition of GO-P significantly affects the blend's morphology, rheological behavior, and mechanical properties. In terms of mechanical characteristics, preblending the modified GO nanosheets with PS increases the blends' strength/strain by $\sim 25\%$ and toughness by $\sim 50\%$ compared to PS/PP uncompatibilized material.

ACKNOWLEDGEMENTS

The research reported was partially supported by the National Science Foundation via EPSCoR OIA-1655740 and CBET-2134564. The authors gratefully acknowledge Kimberly Ivey (Clemson University) for her help and advice.

SUPPORTING INFORMATION

The Supporting Information is available free of charge on the ACS Publications website.

S1. Calculation of surface and interfacial energies. S2. Determination of melt viscosity. S3. Calculation of phase inversion point. S4. Differential Scanning Calorimetry (DSC) results. S4. Mechanical properties of PS/PP blends: experiment and prediction by the rule of mixture. S5. Mechanical properties of PS/PP, PS/PP-POGL, and PS-POGL/PP blends. S6. Morphology of PS/PP-POGL and PS-POGL/PP blends. S7. References

References

- 1. Fried, J. R., *Polymer Science and Technology*. 3rd ed.; Prentice Hall: Upper Saddle River, NJ, 2014; p 1-3.
- 2. <u>https://www.statista.com/topics/7460/plastics-industry-in-the-us/#topicHeader_wrapper</u> (accessed 07/6/2022).
- 3. Ehrenstein, G. W., *Polymeric Materials : Structure, Properties, Applications*. Hanser ; Hanser Gardner Publications: Munich; Cincinnati, OH, 2001; p 278.
- 4. Geyer, R.; Jambeck, J. R.; Law, K. L., Production, Use, and Fate of all Plastics Ever Made. *Sci. Adv.* **2017**, *3* (7), e1700782.
- 5. Lemonick, S., Chemical Solutions for a Chemical Problem. *Chem. Eng. News* **2018**, *96*, 26-29.
- 6. Coates, G. W.; Getzler, Y. D., Chemical Recycling to Monomer for an Ideal, Circular Polymer Economy. *Nat. Rev. Mater.* **2020**.
- 7. Ragaert, K.; Delva, L.; Van Geem, K., Mechanical and Chemical Recycling of Solid Plastic Waste. *Waste Manage.* **2017**, *69*, 24-58.
- 8. Ragaert, K.; Hubo, S.; Delva, L.; Veelaert, L.; Du Bois, E., Upcycling of Contaminated Post-Industrial Polypropylene Waste: A Design from Recycling Case Study. *Polym. Eng. Sci.* **2018**, *58* (4), 528-534.
- 9. Garcia, J. M.; Robertson, M. L., The Future of Plastics Recycling Chemical Advances are Increasing the Proportion of Polymer Waste that can be Recycled. *Science* **2017**, *358* (6365), 870-872.
- 10. Crippa, M.; Morico, B., PET Depolymerization: a Novel Process for Plastic Waste Chemical Recycling. In *Stud. Surf. Sci. Catal.*, Basile, A.; Centi, G.; Falco, M. D.; Iaquaniello, G., Eds. Elsevier: 2019; Vol. 179, pp 215-229.
- 11. Khoonkari, M.; Haghighi, A. H.; Sefidbakht, Y.; Shekoohi, K.; Ghaderian, A., Chemical Recycling of PET Wastes with Different Catalysts. *Int. J. Polym. Sci.* **2015**, *2015*, 124524.
- 12. European Circular Economy Stakeholder Platform: Zero Waste Europe-2019, El Dorado of Chemical Recycling: State of play and policy challenges. https://circulareconomy.europa.eu/platform/sites/default/files/2019_08_29_zwe_study_chemical_recycling.pdf (accessed 04/15/2022).
- 13. Maris, J.; Bourdon, S.; Brossard, J.-M.; Cauret, L.; Fontaine, L.; Montembault, V., Mechanical Recycling: Compatibilization of Mixed Thermoplastic Wastes. *Polym. Degrad. Stab.* **2018**, *147*, 245-266.

- 14. Schyns, Z. O. G.; Shaver, M. P., Mechanical Recycling of Packaging Plastics: A Review. *Macromol. Rapid Commun.* **2021**, *42* (3), 2000415.
- 15. Cao, Y.; Zhang, J.; Feng, J.; Wu, P., Compatibilization of Immiscible Polymer Blends Using Graphene Oxide Sheets. *ACS Nano* **2011**, *5* (7), 5920-5927.
- 16. Koning, C.; Van Duin, M.; Pagnoulle, C.; Jerome, R., Strategies for Compatibilization of Polymer Blends. *Prog. Polym. Sci.* **1998**, *23* (4), 707-757.
- 17. Sperling, L. H., *Introduction to Physical Polymer Science*. Fourth ed.; Wiley-Interscience Hoboken, New Jersey, 2006; p 845.
- 18. Hiemenz, P. C.; Lodge, T., *Polymer Chemistry*. 2nd ed.; CRC Press: Boca Raton, 2007; p 587.
- 19. Utracki, L. A., Compatibilization of Polymer Blends. *Can. J. Chem. Eng.* **2002,** *80* (6), 1008-1016.
- 20. Santos, P.; Pezzin, S. H., Mechanical Properties of Polypropylene Reinforced with Recycled-PET Fibres. *J. Mater. Process. Technol.* **2003**, *143-144*, 517-520.
- 21. Bremner, T.; Rudin, A.; Cook, D. G., Melt Flow Index Values and Molecular Weight Distributions of Commercial Thermoplastics. *J. Appl. Polym. Sci.* **1990**, *41* (78), 1617-1627.
- 22. Marcincin, A.; Jambrich, M., Textile Polypropylene Fibers: Fundamentals. In *Polypropylene : an A-Z reference*, Karger-Kocsis, J., Ed. Kluwer: Dordrecht, 1999; pp 816-820.
- 23. Karacan, I., Structure-Property Relationships in Polypropylene Fibers. In *Polypropylene : an A-Z reference*, Karger-Kocsis, J., Ed. Kluwer: Dordrecht, 1999; pp 783-789.
- 24. De Francesco, A.; Duckett, R. A., Effects of Orientation on Mechanical Properties of Uniaxially Oriented Polystyrene Films. *Polymer* **2004**, *45* (23), 8005-8011.
- 25. Kumar, V.; Singh, R.; Ahuja, I. P. S., Effect of Extrusion Parameters on Primary Recycled ABS: Mechanical, Rheological, Morphological and Thermal Properties. *Mater. Res. Express* **2020**, 7 (1), 015208.
- 26. Soriano, F.; Morales, G.; De León, R. D., Recycling of High Impact Polystyrene in Coextruded Sheet: Influence of the Number of Processing Cycles on the Microstructure and Macroscopic Properties. *Polym. Eng. Sci.* **2006**, *46* (12), 1698-1705.
- 27. Utracki, L. A., On the Viscosity-Concentration Dependence of Immiscible Polymer Blends. *J. Rheol.* **1991,** *35* (8), 1615-1637.
- 28. Brown, S. B., Reactive Compatibilization of Polymer Blends. In *Polymer Blends Handbook*, Utracki, L. A., Ed. Springer Netherlands: 2003; pp 339-415.
- 29. Iyer, S.; Schiraldi, D. A., Role of Ionic Interactions in the Compatibility of Polyester Ionomers with Poly(ethylene terephthalate) and Nylon 6. *J. Polym. Sci., Part B: Polym. Phys.* **2006**, *44* (15), 2091-2103.
- 30. Salzano De Luna, M.; Filippone, G., Effects of Nanoparticles on the Morphology of Immiscible Polymer Blends Challenges and Opportunities. *Eur. Polym. J.* **2016,** *79*, 198-218.
- 31. Taguet, A.; Cassagnau, P.; Lopez-Cuesta, J. M., Structuration, Selective Dispersion and Compatibilizing Effect of (Nano)Fillers in Polymer Blends. *Prog. Polym. Sci.* **2014**, *39* (8), 1526-1563.
- 32. Nazockdast, H., Morphology and Structure of Polymer Blends Containing Nanofillers. In *Encyclopedia of Polymer Blends*, 2016; pp 401-482.
- 33. Tu, C.; Nagata, K.; Yan, S., Influence of Melt-Mixing Processing Sequence on Electrical Conductivity of Polyethylene/Polypropylene Blends Filled with Graphene. *Polym. Bull.* **2016,** *74* (4), 1237-1252.

- 34. Lee, C.; Wei, X.; Kysar, J. W.; Hone, J., Measurement of the Elastic Properties and Intrinsic Strength of Monolayer Graphene. *Science* **2008**, *321* (5887), 385-388.
- 35. Alam, F.; Choosri, M.; Gupta, T. K.; Varadarajan, K. M.; Choi, D.; Kumar, S., Electrical, Mechanical and Thermal Properties of Graphene Nanoplatelets Reinforced UHMWPE Nanocomposites. *Mater. Sci. Eng. B* **2019**, *241*, 82-91.
- 36. Bai, L.; He, S.; Fruehwirth, J. W.; Stein, A.; Macosko, C. W.; Cheng, X., Localizing Graphene at the Interface of Cocontinuous Polymer Blends: Morphology, Rheology, and Conductivity of Cocontinuous Conductive Polymer Composites. *J. Rheol.* **2017**, *61* (4), 575-587.
- 37. Yun, Y. S.; Bae, Y. H.; Kim, D. H.; Lee, J. Y.; Chin, I.-J.; Jin, H.-J., Reinforcing Effects of Adding Alkylated Graphene Oxide to Polypropylene. *Carbon* **2011**, *49* (11), 3553-3559.
- 38. Long, J.; Li, S.; Liang, J.; Wang, Z.; Liang, B., Preparation and Characterization of Graphene Oxide and it Application as a Reinforcement in Polypropylene Composites. *Polym. Compos.* **2018**, *40* (2), 723-729.
- 39. Cho, S.; Kim, M.; Lee, J. S.; Jang, J., Polypropylene/Polyaniline Nanofiber/Reduced Graphene Oxide Nanocomposite with Enhanced Electrical, Dielectric, and Ferroelectric Properties for a High Energy Density Capacitor. *ACS Appl. Mater. Interfaces* **2015**, *7* (40), 22301-14.
- 40. You, F.; Wang, D.; Li, X.; Liu, M.; Dang, Z.-M.; Hu, G.-H., Synthesis of Polypropylene-Grafted Graphene and its Compatibilization Effect on Polypropylene/Polystyrene Blends. *J. Appl. Polym. Sci.* **2014**, *131* (13), n/a-n/a.
- 41. Hao, Y.; Zhao, X.; Dong, J.; Zhang, Q., The Compatibilization Effects of Alkylated-grafted-Graphene Oxide on Polypropylene/Polystyrene Blends. *Int. J. Polym. Sci.* **2017**, 2017, 1-11.
- 42. Amani, M.; Sharif, M.; Kashkooli, A.; Rahnama, N.; Fazli, A., Effect of Mixing Conditions on the Selective Localization of Graphite Oxide and The Properties of Polyethylene/High-Impact Polystyrene/Graphite Oxide Nanocomposite Blends. *RSC Advances* **2015**, *5* (95), 77723-77733.
- 43. Borodinov, N.; Gil, D.; Savchak, M.; Gross, C. E.; Yadavalli, N. S.; Ma, R.; Tsukruk, V. V.; Minko, S.; Vertegel, A.; Luzinov, I., En Route to Practicality of the Polymer Grafting Technology: One-Step Interfacial Modification with Amphiphilic Molecular Brushes. *ACS Appl. Mater. Interfaces* **2018**, *10* (16), 13941-13952.
- 44. https://www.goographene.com/store/p32/2000_ML_Single-Layer Graphene Oxide Aqueous Dispersion.html (accessed 04/15/2022).
- 45. Abbasi, F.; Shojaei, D. A.; Bellah, S. M., The Compatibilization Effect of Exfoliated Graphene on Rheology, Morphology, and Mechanical and Thermal Properties of Immiscible Polypropylene/Polystyrene (PP/PS) Polymer Blends. *J. Thermoplast. Compos. Mater.* **2018**, *32* (10), 1378-1392.
- 46. Luzinov, I.; Xi, K.; Pagnoulle, C.; Huynh-Ba, G.; Jérôme, R., Composition Effect on the Core–Shell Morphology and Mechanical Properties of Ternary Polystyrene/Styrene–Butadiene Rubber/Polyethylene Blends. *Polymer* **1999**, *40* (10), 2511-2520.
- 47. Wu, S., Calculation of Interfacial Tension in Polymer Systems. J. Polym. Sci., Part C: Polym. Symp. 1971, 34, 19-30.
- 48. Biscerano, J., *Prediction of Polymer Properties*. Third Edition ed.; Marcel Dekker: 2002.
- 49. Luzinov, I.; Xi, K.; Pagnoulle, C.; Huynh-Ba, G.; Jerome, R., Composition Effect on the Core-Shell Morphology and Mechanical Properties of Ternary Polystyrene/Styrene Butadiene Rubber Polyethylene Blends. *Polymer* **1999**, *40* (10), 2511-2520.

- 50. Sumita, M.; Sakata, K.; Asai, S.; Miyasaka, K.; Nakagawa, H., Dispersion of Fillers and the Electrical Conductivity of Polymer Blends Filled With Carbon Black. *Polym. Bull.* **1991,** *25* (2), 265-271.
- 51. Zdyrko, B.; Luzinov, I., Polymer Brushes by the "Grafting to" Method. *Macromol. Rapid Commun.* **2011**, *32* (12), 859-869.
- 52. Benaglia, M.; Alberti, A.; Giorgini, L.; Magnoni, F.; Tozzi, S., Poly(glycidyl methacrylate): a Highly Versatile Polymeric Building Block for Post-Polymerization Modifications. *Polym. Chem.* **2013**, *4* (1), 124-132.
- 53. Scheibe, P.; Barz, M.; Hemmelmann, M.; Zentel, R., Langmuir-Blodgett Films of Biocompatible Poly(HPMA)-block-Poly(lauryl methacrylate) and Poly(HPMA)-random-Poly(lauryl methacrylate): Influence of Polymer Structure on Membrane Formation and Stability. *Langmuir* **2010**, *26* (8), 5661-9.
- 54. Panyukov, S.; Zhulina, E. B.; Sheiko, S. S.; Randall, G. C.; Brock, J.; Rubinstein, M., Tension Amplification in Molecular Brushes in Solutions and on Substrates. *J. Phys. Chem. B* **2009**, *113* (12), 3750-3768.
- 55. Tu, S. D.; Choudhury, C. K.; Luzinov, I.; Kuksenok, O., Recent Advances towards Applications of Molecular Bottlebrushes and their Conjugates. *Curr. Opin. Solid State Mat. Sci.* **2019**, *23* (1), 50-61.
- 56. Li, Z.; Tang, M.; Liang, S.; Zhang, M.; Biesold, G. M.; He, Y.; Hao, S.-M.; Choi, W.; Liu, Y.; Peng, J.; Lin, Z., Bottlebrush Polymers: From Controlled Synthesis, Self-Assembly, Properties to Applications. *Prog. Polym. Sci.* **2021**, *116*, 101387.
- 57. Kim, H.; Abdala, A. A.; Macosko, C. W., Graphene/Polymer Nanocomposites. *Macromolecules* **2010**, *43* (16), 6515-6530.
- 58. Vermant, J.; Ceccia, S.; Dolgovskij, M. K.; Maffettone, P. L.; Macosko, C. W., Quantifying Dispersion of Layered Nanocomposites via Melt Rheology. *J. Rheol.* **2007**, *51* (3), 429-450.
- 59. Utracki, L. A.; Lyngaae-Jørgensen, J., Dynamic Melt Flow of Nanocomposites Based on Poly-e-Caprolactam. *Rheol. Acta* **2002**, *41* (5), 394-407.
- 60. Pukanszky, B., Particulate Filled Polypropylene Composites. In *Polypropylene : an A-Z reference*, Karger-Kocsis, J., Ed. Kluwer: Dordrecht, 1999; pp 574-580.
- 61. Utracki, L. A.; Luciani, A., Rheology of Polypropylene. In *Polypropylene : an A-Z reference*, Karger-Kocsis, J., Ed. Kluwer: Dordrecht, 1999; pp 715-720.
- 62. Utracki, L. A.; Wilkie, C. A., *Polymer Blends Handbook*. 2nd ed.; Springer: Dordrecht, 2014.
- 63. Mustafa, S. J. S.; Nor Azlan, M. R.; Ahmad Fuad, M. Y.; Mohd Ishak, Z. A.; Ishiaku, U. S., Polypropylene/Polystyrene Blends: Preliminary Studies for Compatibilization by Aromatic-Grafted Polypropylene. *J. Appl. Polym. Sci.* **2001,** *82* (2), 428-434.
- 64. Omonov, T. S.; Harrats, C.; Moldenaers, P.; Groeninckx, G., Phase continuity Detection and Phase Inversion Phenomena in Immiscible Polypropylene/Polystyrene Blends with Different Viscosity Ratios. *Polymer* **2007**, *48* (20), 5917-5927.
- 65. Paul, D. R.; Barlow, J. W., Polymer Blends. J. Macromol. Sci. C 1980, 18 (1), 109-168.
- 66. Wu, S. H., Formation of Dispersed Phase in Incompatible Polymer Blends Interfacial and Rheological Effects. *Polym. Eng. Sci.* **1987,** *27* (5), 335-343.
- 67. Shen, L.; Zhang, L.; Wang, K.; Miao, L.; Lan, Q.; Jiang, K.; Lu, H.; Li, M.; Li, Y.; Shen, B.; Zheng, W., Analysis of Oxidation Degree of Graphite Oxide and Chemical Structure of Corresponding Reduced Graphite Oxide by Selecting Different-Sized Original Graphite. *RSC Advances* **2018**, *8* (31), 17209-17217.

- 68. Hu, K.; Gupta, M. K.; Kulkarni, D. D.; Tsukruk, V. V., Ultra-Robust Graphene Oxide-Silk Fibroin Nanocomposite Membranes. *Adv. Mater.* **2013**, *25* (16), 2301-2307.
- 69. Gomez-Navarro, C.; Burghard, M.; Kern, K., Elastic Properties of Chemically Derived Single Graphene Sheets. *Nano Lett.* **2008**, *8* (7), 2045-2049.
- 70. Suk, J. W.; Piner, R. D.; An, J.; Ruoff, R. S., Mechanical Properties of Monolayer Graphene Oxide. *ACS Nano* **2010**, *4* (11), 6557-6564.

FOR TABLE OF CONTENT ONLY.

